# Supplementary Information

# Photo-Exfoliation of a Highly Photo-Responsive Two-Dimensional Metal-Organic Framework

Jian Xie,[a, †] Yaxing Wang, [a, †] Duo, Zhang, [a, †] Chengyu Liang, [a] Wei Liu,[a] Yu Chong,[a] Xuemiao Yin,[a] Yugang Zhang,[a] Daxiang Gui,[a] Lanhua Chen,[a] Wei Tong, [b] Zhiyong Liu,[a] Juan Diwu,[a] Zhifang Chai, [a] and Shuao Wang*, [a]

[a]State Key Laboratory of Radiation Medicine and Protection, School for Radiological and interdisciplinary Sciences (RAD-X) and Collaborative Innovation Centre of Radiation Medicine of Jiangsu Higher Education Institutions, Soochow University, Suzhou 215123, China

[b]High Magnetic Field Laboratory, Chinese Academy of Sciences, Hefei, Anhui, 230031, China

## S1. Experimental section.

***Caution! Uranium is a radioactive and chemically toxic element. Although depleted uranium was used in this study, standard procedure for handling radioactive materials should be followed.***

**Reagents.** $UO_2(NO_3)_2 \cdot 6H_2O$, $H_2ox \cdot 2H_2O$ (oxalic acid), phen (1,10-phenanthroline), and deionized water were used as received from commercial suppliers without further purification.

**Synthesis of $[Hphen]_2[(UO_2)_2(ox)_3]$ (1).** A mixture of $UO_2(NO_3)_2 \cdot 6H_2O$ (50.2 mg, 0.1 mmol), $H_2ox \cdot 2H_2O$ (126.0 mg, 1.0 mmol), phen (19.5 mg 0.1 mmol), and deionized water (200 μL) were loaded into 10 mL vials. The vials were then sealed and heated to 100 °C for 12 h and cooled to room temperature under ambient condition. Reddish-brown block like crystals of **1** were isolated after being washed with deionized water and allowed to air-dry at room temperature. The phase purity was confirmed by the powder XRD analyses, which are shown in Fig. S2.

## S2. Characterizations.

Powder X-ray diffraction (PXRD) data were collected from 5 to 50° with a step of 0.02° and the time for data collection was 0.5 s on a Bruker D8 Advance diffractometer with Cu Kα radiation (λ=1.54056 Å) and a Lynxeye one - Dimensional detector. Single crystal data collection was performed on a Bruker D8-Venture diffractometer with a Turbo X-ray Source (Mo–Kα radiation, λ = 0.71073 Å) adopting the direct-drive rotating anode technique and a CMOS detector at room temperature. The data frames were collected using the program APEX2 and processed using the program SAINT routine in APEX2. The ATR/FTIR spectra of the sample without KBr were recorded in the range of 4000-400 $cm^{-1}$ by a Thermo Nicolet iS 50 spectrometer. The single crystal solid-state photoluminescence and UV-vis absorption spectra were recorded on a Craic Technologoes microspectrophotometer; Crystals

were placed on quartz slide, and data was collected after auto-set optimization. When the 365 nm excitation light was selected, an optical filter masking signal below 420 nm was applied in order to mask the interference of excitation light. Thermalgravimetric (TG - DSC) analysis was carried out on a NETZSCH STA 449 F3 jupiter instrument in the range of 30 - 900 °C under a nitrogen flow at a heating rate of 10 °C/ min. The electron paramagnetic resonance (EPR) data for the 1 hour UV irradiated sample was recorded with a Bruker EMXplus 10/12 EPR spectrometer equipped with an Oxford Instruments EPR901 liquid helium continuous-flow cryostat fitted with a super-high-Q cavity. The magnetic field was measured by a Hall probe calibrated with the 1,3-bisdiphenylene-2-phenylallyl EPR signal and a Bruker ER 036TM teslameter. The microwave frequency was measured with an internal frequency counter. The temperature was controlled with an Oxford Instruments ITC503S temperature controller. The spectra were acquired with a sweep width of 2000 G, a frequency of 9.383303 GHz, a modulation amplitude of 5 G, a modulation frequency of 100 kHz, and at temperature of 110 K. Scanning electron microscopy images and energy-dispersive spectroscopy data (SEM/EDS) were recorded on a FEI Quanta 200FEG Scanning Electron Microscope with the energy of the electron beam being 30 keV. Samples were mounted directly on the carbon conductive tape with Au coating.

## S3. X-ray crystallography.

**Table S1.** Crystallographic data for **1** (nonirradiated and a 20 min UV irradiated sample).

| | Nonirradiated | Irradiated |
|---|---|---|
| Formula | $[Hphen]_2[(UO_2)_2(ox)_3]$ | $[Hphen]_2[(UO_2)_2(ox)_3]$ |
| $Mr$ (g mol$^{-1}$) | 2296.80 | 2296.80 |
| Crystal system | monoclinic | monoclinic |
| Space group | $P2_1/c$ | $P2_1/c$ |
| $a$ (Å) | 7.1196(4) | 7.219(2) |
| $b$ (Å) | 11.8468(7) | 11.787(3) |
| $c$ (Å) | 18.6262(11) | 18.586(5) |
| $\alpha$ | 90 | 90 |
| $\beta$ | 98.714(2) | 98.556(7) |
| $\gamma$ | 90 | 90 |
| $V$ (Å$^3$) | 1552.88(16) | 1563.9(7) |
| $Z$ | 1 | 1 |
| $D_c$ (g cm$^{-3}$) | 2.456 | 2.439 |
| $\mu$ (mm$^{-1}$) | 10.502 | 16.673 |
| $F$ (000) | 1040.0 | 1040.0 |
| T (K) | 298 | 298 |
| GOF on $F^2$ | 1.215 | 1.040 |
| R1,[a] wR2[b] ($I>2\sigma(I)$) | 0.0223, 0.0485 | 0.0608, 0.0981 |
| R1,[a] wR2[b] (all data) | 0.0306, 0.0502 | 0.1434, 0.1181 |

[a] $R_1 = \Sigma||F_o|-|F_c||/\Sigma|F_o|$. [b] $wR_2=[\Sigma w(F_o^2-F_c^2)^2/\Sigma w(F_o^2)^2]^{1/2}$

## S4. Mechanism of photoluminescence in 1.

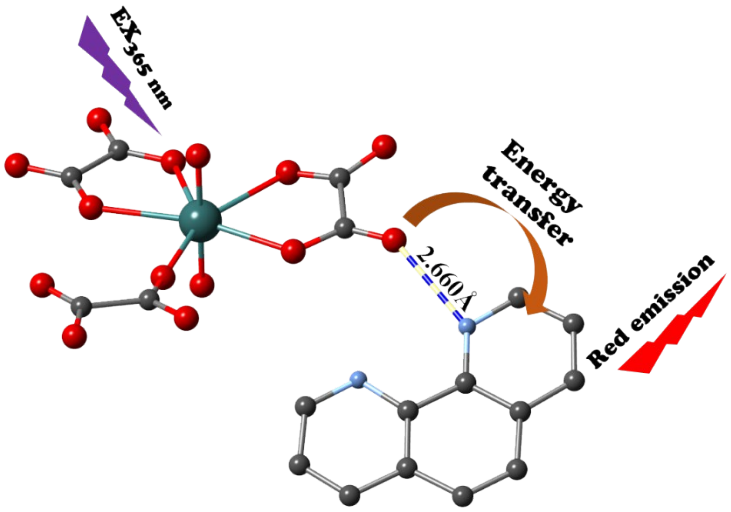


**Fig. S1.** Mechanism of photoluminescence in **1**. Interestingly, as shown in Figure 2c, the photoluminescence spectrum of **1** measured under $\lambda_{ex}$ = 365 nm at ambient temperature exhibits only two emission bands ($\lambda_{em}$ = 592, 655 nm) with the absence of the characteristic emission bands of the uranyl(VI). In order to explain this infrequent optical behavior, we carefully analyzed the structural features in detail. As shown in Figure S1, the nearest O···N distance between adjacent electron-rich carboxylate O atom of the ox and the electron-deficient N atom of phen is 2.660 Å. Therefore, the extremely close distance between electron donor and acceptor plays a key role in offering a pathway for efficient energy transfer from uranyl to phen.

## S5. Powder X-ray diffraction (PXRD).

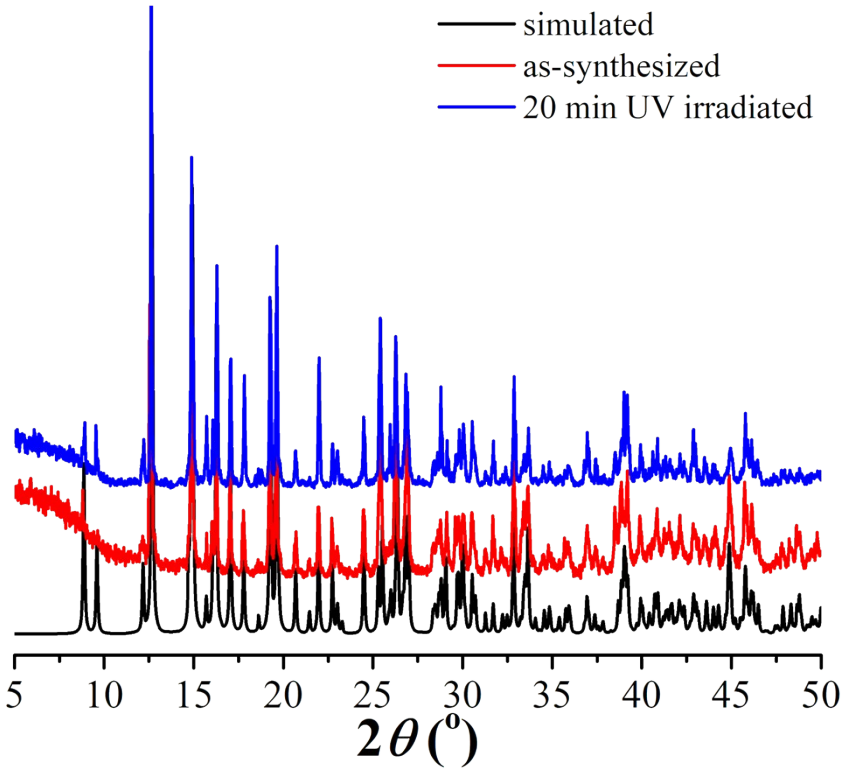


**Fig. S2.** PXRD patterns for simulated, as-synthesized, and UV irradiated samples.

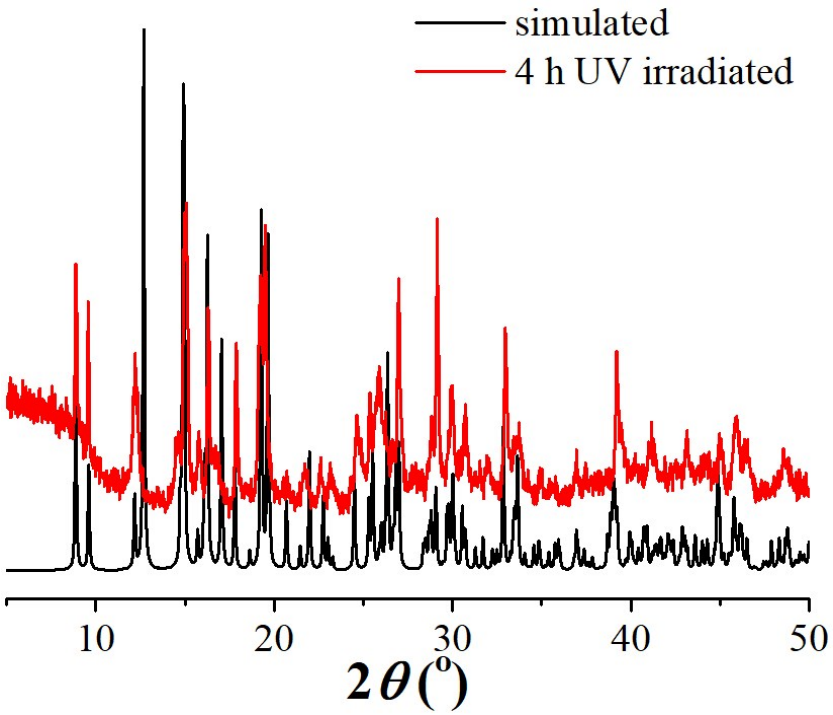


**Fig. S3.** PXRD patterns for simulated, 4 h UV irradiated samples.

## S6. FTIR spectra.

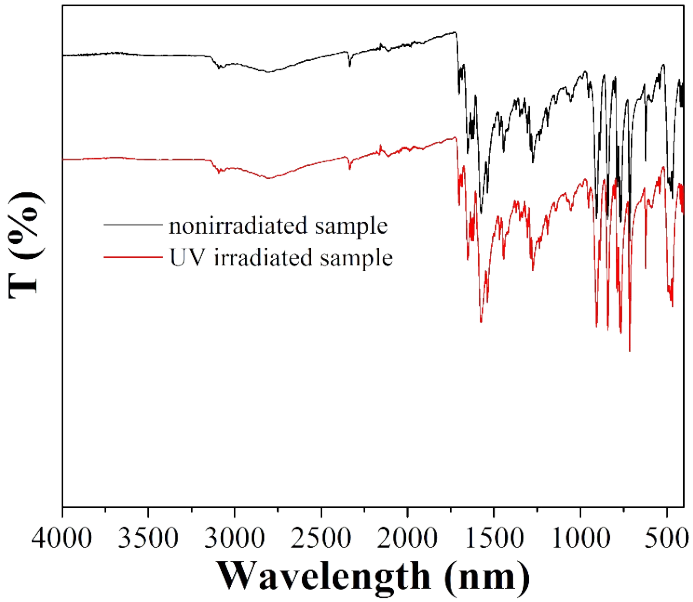


**Fig. S4.** FTIR spectra for the nonirradiated and a UV irradiated sample.

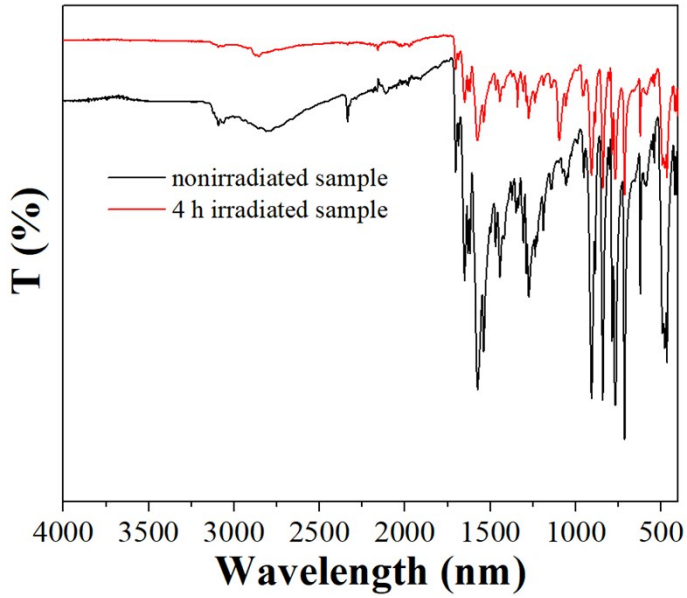


**Fig. S5.** FTIR spectra for the nonirradiated and a 4 h UV irradiated sample.

## S7. EPR measurement.

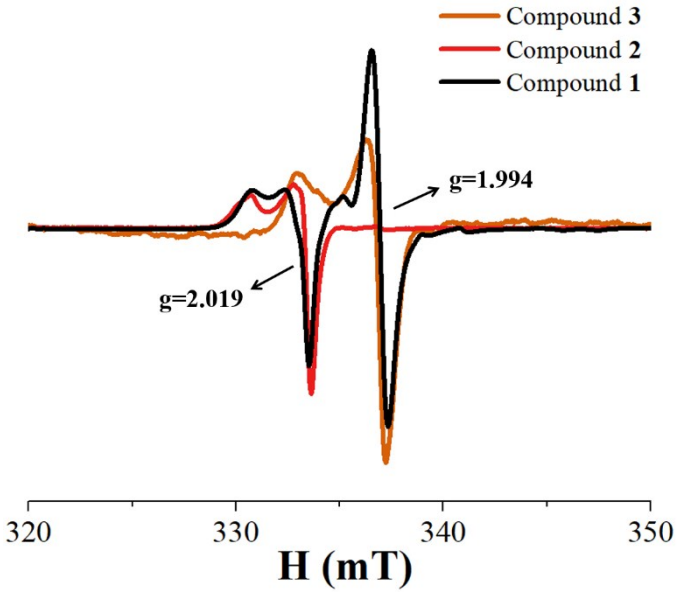


**Fig. S6.** EPR spectra for UV irradiated compound **1**, compound **2**, and compound **3**.

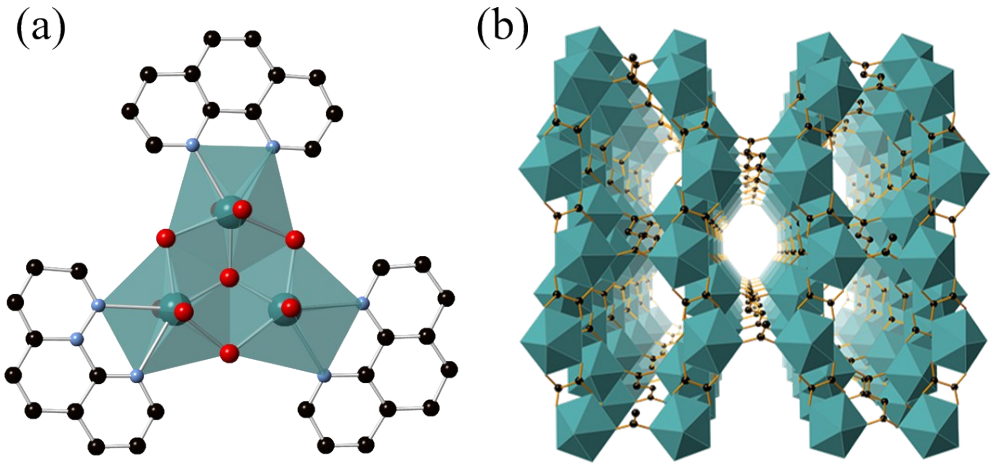


**Fig. S7.** Crystal structure of (a) compound **2** and (b) compound **3**. Color scheme: U: turquoise; O: red; C: black; N: blue. H atoms are omitted for clarity. In order to investigate the radical species producing in compound **1** after UV irradiation, we selected compound **2**, $[(phen)\cdot(OH)]\cdot[(UO_2)_3(O)(OH)_3(phen)_3]$ (phen=1,10-phenanthroline, unpublished compound), and compound **3,** $(TMA)_2[(UO_2)_4(ox)_4L]$ ($TMA^+$=tetramethylammonium cation, ox=oxalate, L=succinate)[1] as the controls which consist of phen and ox, respectively. As shown in Figure S6, the g value of

radical signals measured in UV irradiated compound **2** and **3** are 2.019 and 1.994, respectively, indicating that the signal peak with g value of 2.019 is $[phen]^{+\bullet}$ radical signal and the signal peak with g value of 1.994 is $[ox]^{2-\bullet}$ radical signal. Obviously, as shown in Figure S6, there are two types of radical signals involved in the EPR spectrum of UV irradiated compound **1**, which coincide with those in UV irradiated compound **2** and **3**, respectively. Therefore, both $[ox]^{2-\bullet}$ radical and $[phen]^{+\bullet}$ radical are involved in the UV irradiated sample of compound **1**.

## S8. Radical stability measurement.

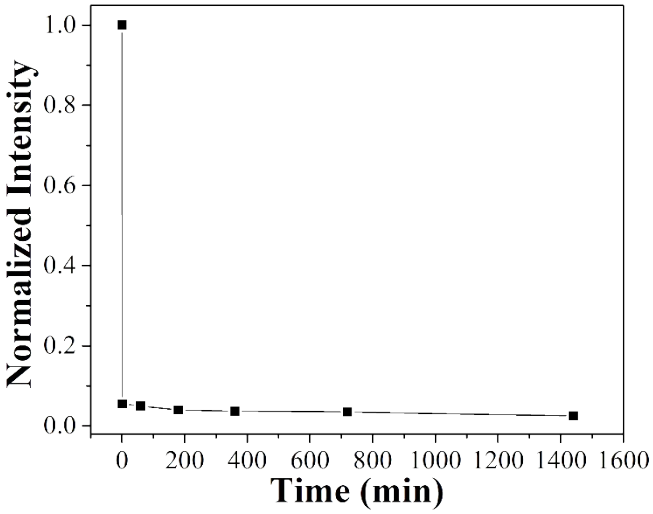


**Fig. S8.** The stability measurement of UV radiation induced radicals. The quenched emission intensity is not recovered change as a function of time indicating the radicals are trapped and stabilized in the structure of **1**.

## S9. UV detection experiment.

As shown in Figure 3a, with the increasing UV radiation dosages, the luminescence intensity of **1** decreased sharply without obvious transformation of characteristic peaks. Noticeably, the emission of **1** was totally quenched after $3.4\times10^{-2}$ mJ UV irradiation (exposure time = 68 s). The emission intensity vs. UV radiation dosage curve in the low-dose range (0–0.002 mJ) can be fitted in a linear relationship (y=21635.4x+3.5, inset of Figure 3b). The detection limit was determined by the following equations[2]:

$$3\sigma/\text{slope} \qquad (1)$$

$$\sigma = 100 \times (I_{SE}/I_0) \qquad (2)$$

where $I_{SE}$ is the standard error of the photoluminescence intensity measurement, as determined by the baseline measurement of the blank sample monitored at 592 nm, and $I_0$ is the measured photoluminescence intensity of **1** with no UV irradiation. The slope was gained from the linear fit of the UV radiation dosage dependent photoluminescence intensity (monitored at 592 nm) curve in the low-dose region (inset of 3b).

## S10. SEM image of UV irradiated crystals of 1.

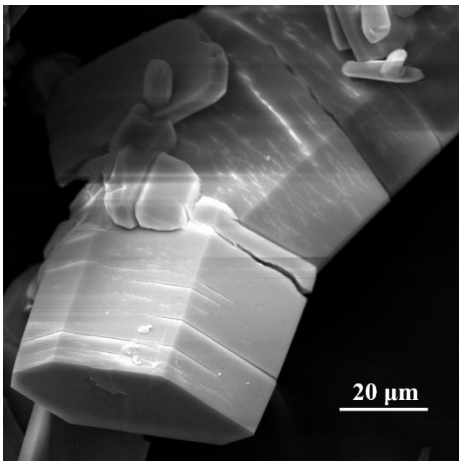


**Fig. S9.** SEM image of UV irradiated crystals of **1**.

## S11. AFM image of 2D MOF nanosheets and their height distribution histograms.

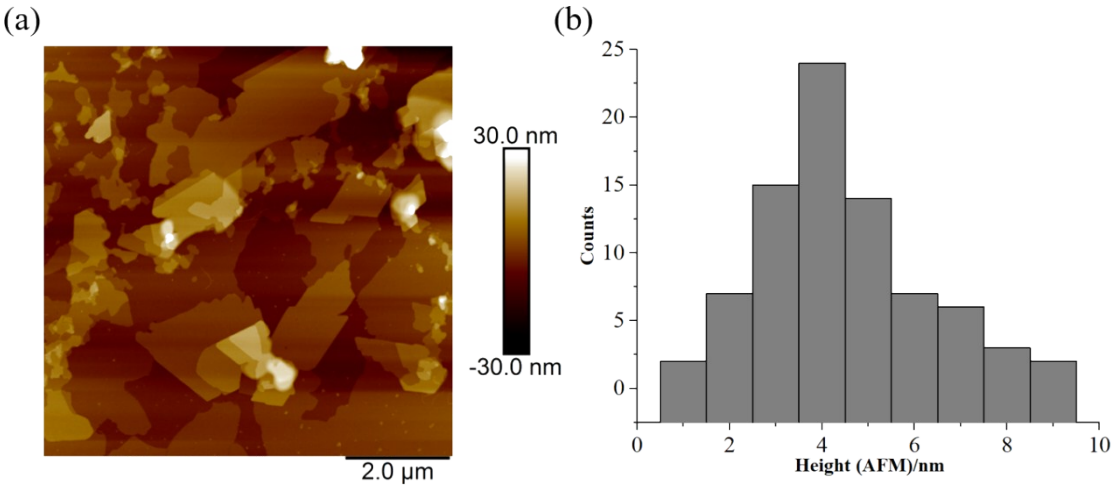


**Fig. S10.** (a) AFM image of 2D MOF nanosheets and (b) their height distribution histograms using~80 platelets.

## S12. UV-vis absorption spectrum.

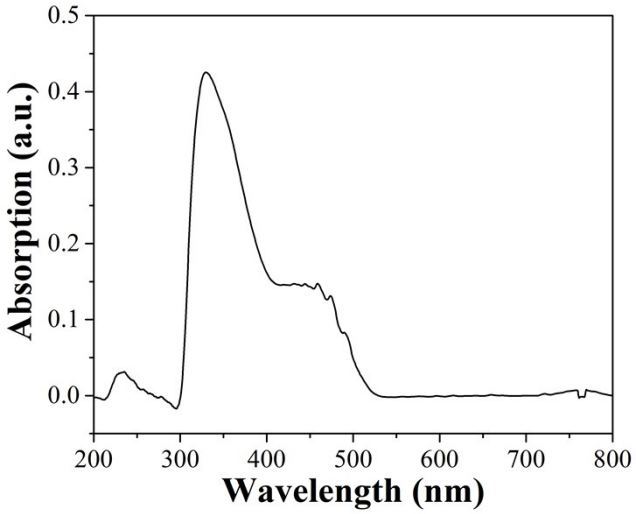


**Fig. S11.** The UV-vis absorption spectrum of **1** at 298 K.

## S13. SEM-EDS analysis.

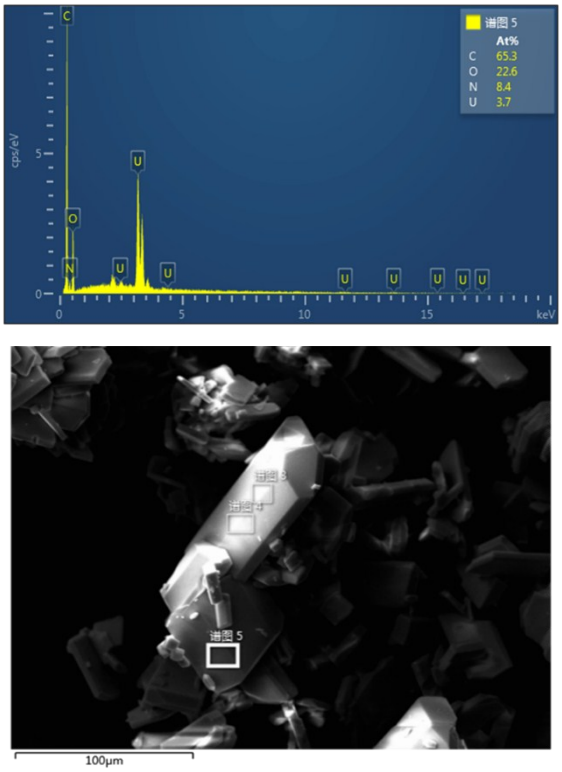


**Fig. S12.** EDS (top) and SEM (bottom) images of compound **1**.

## S14. Thermogravimetric analysis.

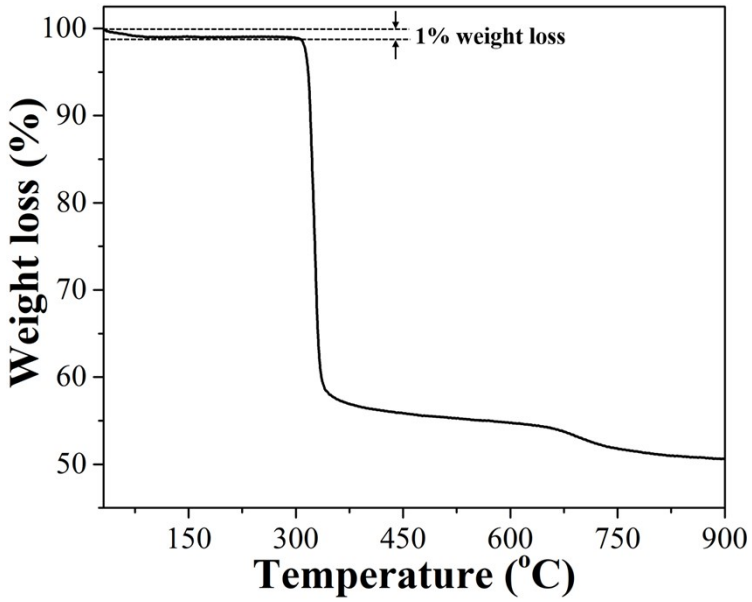


**Fig. S13.** The thermogravimetric analysis data showing **1** is thermally stable up to ca. 306 °C. In 30-300 degree region, the weight loss is 1%, indicating water molecules remove during the heating process.

## S15. Bond distance summary

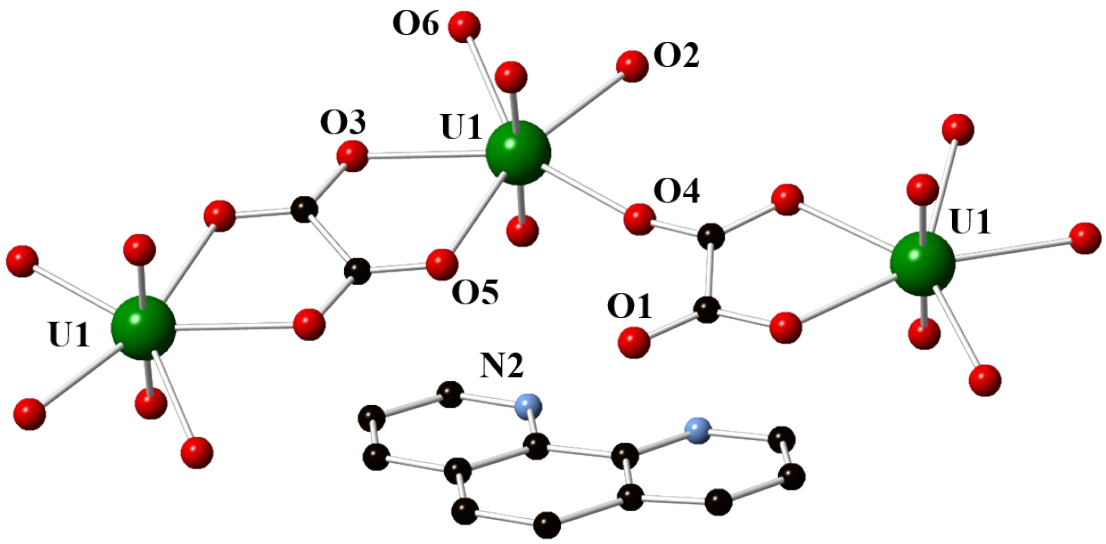


**Fig. S14.** Depiction of a structural fragment of **1** containing arrangement of uranyl, ox groups and phen.

**Table S2.** The distance variation of U-O, U-U, N2-O1 and phen-phen of crystal **1**.

| Bonds | Bond length (Å) (before) | Bond length (Å) (after) | Δd (Å) |
|---|---|---|---|
| U1-O2 | 2.337(2) | 2.335(7) | -0.002 |
| U1-O3 | 2.442(2) | 2.442(7) | 0 |
| U1-O4 | 2.32(2) | 2.286(8) | -0.034 |
| U1-O5 | 2.447(2) | 2.438(6) | -0.009 |
| U1-O6 | 2.42(2) | 2.406(7) | -0.014 |
| Sum | 11.966 | 11.907 | -0.059 |
| Average | 2.3932 | 2.3814 | -0.0118 |
| | | | |
| U-U | 6.348 | 6.336 | -0.012 |
| U-U | 6.679 | 6.652 | -0.027 |
| | | | |
| N2-O1 | 2.672 | 2.693 | 0.021 |

## S16. Photoluminescence decay.

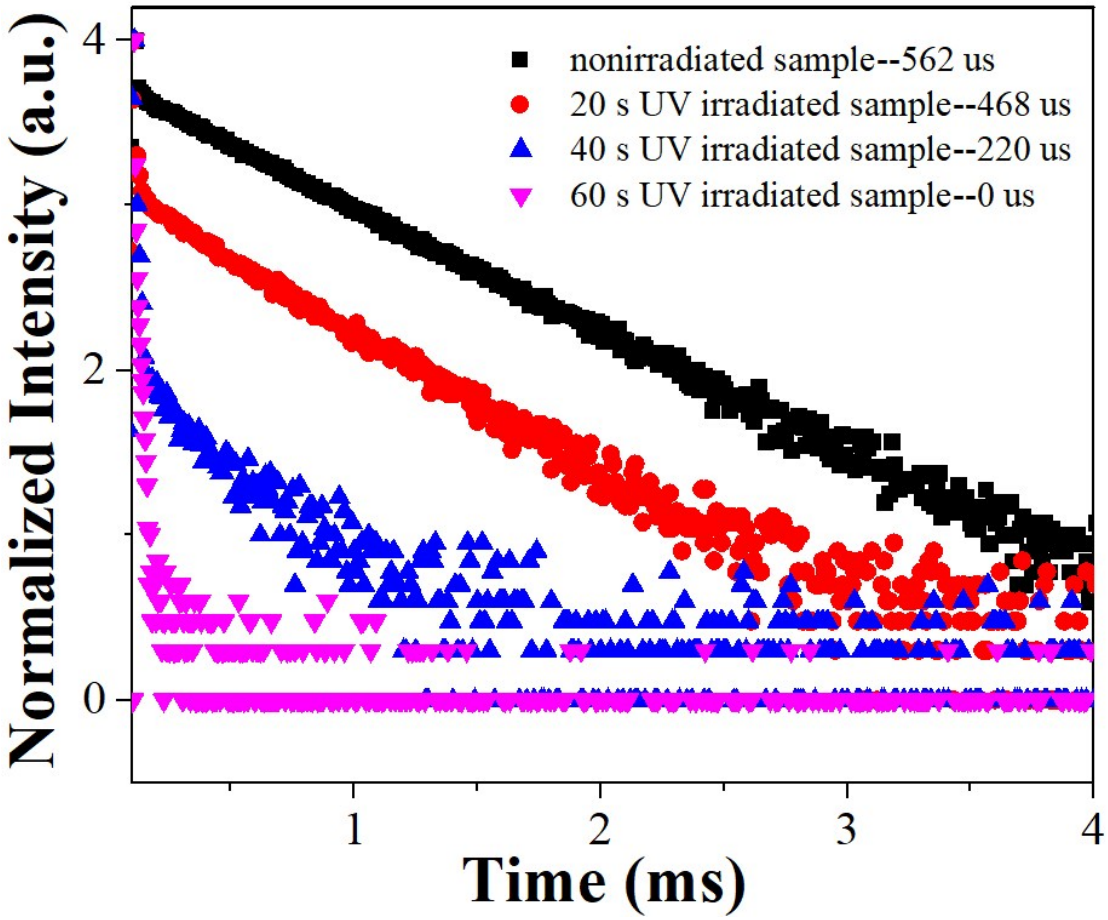


**Fig. S15.** Photoluminescence decay spectrum of nonirradiated sample and 20 s, 40 s, 60 s UV irradiated samples. The lifetime was calculated to be 562 μs, 468 μs, 220 μs and 0 μs, respectively.

## Reference:

(1) J. Xie, Y. X. Wang, W. Liu, X. M. Yin, L. H. Chen, Y. M. Zou, J. Diwu, Z. F. Chai, T. E. Albrecht-Schmitt, G. K. Liu, S. A. Wang, *Angew. Chem. Int. Ed.* 2017, **56**, 7500-7504.

(2) J. M. Han, M. Xu, B. Wang, N. Wu, X. M. Yang, H. R. Yang, B. J. Salter, L. Zang, *J. Am. Chem. Soc.,* 2014, **136**, 5090-5096.